Wavelength Dependence of Nitrate Radical Quantum Yield from Peroxyacetyl Nitrate Photolysis: Experimental and Theoretical Studies

Bradley A. Flowers* and John F. Stanton

Department of Chemistry and Biochemistry, The University of Texas at Austin, Austin, Texas 78712

William R. Simpson

Department of Chemistry and Geophysical Institute, University of Alaska, Fairbanks, Fairbanks, Alaska 99775-6160

Received: June 23, 2007; In Final Form: August 31, 2007

The photolysis wavelength dependence of the nitrate radical quantum yield for peroxyacetyl nitrate ($CH_3C(O)OONO_2$, PAN) is investigated. The wavelength range used in this work is between 289 and 312 nm, which mimics the overlap of the solar flux available in the atmosphere and PAN's absorption cross section. We find the nitrate radical quantum yield from PAN photolysis to be essentially invariant; $\Phi_{NO_3}^{PAN} = 0.30 \pm 0.07$ ($\pm 2\sigma$) in this region. The excited states involved in PAN photolysis are also investigated using *ab initio* calculations. In addition to PAN, calculations on peroxy nitric acid ($HOONO_2$, PNA) are performed to examine general photochemical properties of the $-OONO_2$ chromophore. Equation of motion coupled cluster calculations (EOM-CCSD) are used to examine excited state energy gradients for the internal coordinates, oscillator strengths, and transition energies for the $n \rightarrow \pi^*$ transitions responsible for the photolysis of both PNA and PAN. We find in both molecules, photodissociation of both O−O and O−N bonds occurs via excitation to predissociative electronic excited states and subsequent redistribution of that energy as opposed to directly dissociative excitations. Comparison and contrast between experimental and theoretical studies of $HOONO_2$ and PAN photochemistry from this and other work provide unique insight on the photochemistry of these species in the atmosphere.

I. Introduction

Photolysis properties of peroxy nitrate ($X-OONO_2$) species have become the subject of several experimental and theoretical studies due in part to their importance as NO_2 and peroxyl radical reservoirs in the atmosphere. Both peroxy nitric acid ($HOONO_2$, PNA) and peroxyacetyl nitrate ($CH_3C(O)OONO_2$, PAN) are reservoirs for NO_2 and peroxy radicals (HO_2 and $CH_3C(O)O_2$).[1−5] Peroxy nitrates (most notably PAN) form in polluted regions and can undergo long-range transport. Their subsequent decomposition, through either thermal or photolytic means, releases HO_2, RO_2, and NO_2, which impacts ozone levels in regions far from the source of the pollution. For both PAN and PNA, the majority of photolysis and all thermolysis results in the production of peroxyl radicals and NO_2, shown by processes 1 and 3. Below 248 nm, the NO_2 and NO_3 producing channels dominate the dissociation of both PAN and PNA for solar photolysis.[6−11] The photolysis branching ratios for PAN and PNA are crucial to accurately understanding the release of NO_2 and peroxyl radicals from these reservoirs.

$$HOONO_2 \rightarrow HO_2 + NO_2 \quad (1)$$

$$HOONO_2 \rightarrow HO + NO_3 \quad (2)$$

$$CH_3C(O)OONO_2 \rightarrow CH_3C(O)O_2 + NO_2 \quad (3)$$

$$CH_3C(O)OONO_2 \rightarrow CH_3C(O)O + NO_3 \quad (4)$$

Initial results indicate quite different photochemical quantum yields for PAN and PNA. In the case of PNA, a very recent study by Jimenez et al.[6] at 193, 248, and 308 nm shows $\Phi_{NO_3}^{PNA} = 0.35 \pm 0.09$, 0.08 ± 0.04, and 0.05 ± 0.02 respectively. At 248 nm, $\Phi_{NO_3}^{PNA}$ was also inferred from a measurement of $\Phi_{OH}^{PNA} = 0.34 \pm 0.16$ by MacLeod et al.[3]

The trend in $\Phi_{NO_3}^{PNA}$ indicates (2) is wavelength independent below 248 nm and that (2) is a minor process in $HOONO_2$ photolysis. However, the trend for $\Phi_{NO_3}^{PAN}$ appears markedly different. Both $-NO_2$ and C=O chromophores absorb in the UV, further complicating the dissociative processes within PAN*. For PAN, $\Phi_{NO_3}^{PAN}$ has been measured at 248 nm to be 0.20 ± 0.04,[8] 0.31 ± 0.08 at 289 nm,[11] and 0.41 ± 0.10 at 308 nm.[8] The bond energies for (3) and (4) are much less certain than for the PNA dissociation reactions (1) and (2).[12−14] We estimate $\Delta_R H(4)$ to be at least 10 ± 7 kcal mol^{-1} higher in energy than $\Delta_R H(3)$ at 298 K, whereas the difference between the same dissociations for $HOONO_2$ is 15 ± 1 kcal mol^{-1}. As the photolysis energy decreases, the NO_3 quantum yield apparently increases. This trend, if confirmed, would be remarkable because it would imply as photolysis energy decreases, dissociation via (4) increases per photon absorbed. Yet, at 308 nm, the results of Harwood et al. are sufficiently uncertain to allow for an independent relationship between photolysis wavelength and NO_3 quantum yield. Beyond 308 nm

* Current address: Department of Chemistry and Biochemistry, University of Colorado at Boulder, Boulder, CO 80305-0219. Electronic mail: bradley.flowers@colorado.edu.

10.1021/jp0749118 CCC: $37.00
Published on Web 10/24/2007

there is no information for $\Phi_{NO_3}^{PAN}$. Clearly the trend remains in doubt for PAN at atmospherically relevant photolysis wavelengths. Although the current results at 289 and 308 nm could agree, it is desirable to confirm the relationship between photolysis wavelength and $\Phi_{NO_3}^{PAN}$. To investigate the wavelength dependence of (4), we have measured the nitrate radical quantum yield at 289, 294, 299, 308, and 312 nm, using cavity ring-down absorption spectroscopy (CRDS) to detect NO_3.

In addition to quantum yield experiments, *ab initio* calculations have been used to study the ground and excited states involved in PNA and PAN photolysis. Previous studies of both PAN and PNA photochemistry indicate two n $\rightarrow \pi^*$ transitions on $-NO_2$ chromophore are dissociative transitions.[7,15] The results reported in Roehl et al.[7] predict two singlet excited states for $HOONO_2$ with vertical excitation energies near 5 eV using both complete active space self-consistent field (CASSCF) and multireference configuration interaction (MRCI) methods. In a second study, Francisco and Li[15] identify three excited states involved in the UV absorption spectra of PAN, the lowest two states were $-NO_2$ n $\rightarrow \pi^*$ excitations, and the third state was correlated to an n $\rightarrow \pi^*$ transition on the C=O moiety of PAN. Their methodology was extended to include equation of motion coupled cluster (EOM-CC) calculations for PAN. These calculations indicate that the third transition has the stronger transition dipole and that accounts for the observed difference in the absorption spectrum of PAN relative to PNA. We have also used EOM-CC methods to calculate the vertical excitation energies but for three PNA excited states and four excited states for PAN. We include oscillator strengths for the predicted transitions in our analysis. Additionally, we calculate excited state energy gradients for the internal coordinate displacements for PNA and PAN singlet excited states. From these calculations, we are able to estimate the instantaneous force along the internal coordinates while the molecule is in its vertically excited state and attempt to understand the basis for the observed differences between PAN and PNA photodissociation quantum yields.

II. Method

A detailed discussion of our experimental procedure has been recently published.[11] A brief description is given below. A frequency doubled dye laser is used to photolyze either PAN or the N_2O_5 reference gas, and the NO_3 produced is detected via CRDS using light from a second dye laser. Both photolysis and probe beams are pumped by the second harmonic output of a Nd:YAG laser (532 nm). For the photolysis wavelengths used in this study, Kiton 620 (294, 299 nm) and Sulforhodamine 640 (308, 312 nm) laser dyes were used in addition to Rhodamine 6G (289 nm). A mechanical shutter operated at 1 Hz in the beam path modulates photolysis. The CRDS beam was generated by pumping the DCM laser dye. Two high-reflectivity mirrors were aligned to form the optical cavity. An avalanche photodiode detected the ring-down signal from the optical cavity. Baseline ring-down times (τ_{BL}) were observed up to 40 μs. The probe laser is scanned between 655 and 669 nm to detect the ($^2\tilde{B} \leftarrow {}^2\tilde{X}$) NO_3 transition centered at 662 nm. In the presence of the photolysis laser, the ring-down time (τ_{ON}) decays faster than τ_{BL} due to additional absorption by photolytic NO_3. Ring-down times were recorded for both photolysis states and subtracted from one another to extract the photolytic NO_3 concentration. The raw photolytic difference fit to a reference spectrum[16] to obtain the photolytic NO_3 number density.

$$\Delta r = \frac{1}{c}\left(\frac{1}{\tau_{ON}} - \frac{1}{\tau_{BL}}\right)\frac{l}{l_s} = \Delta[NO_3]\sigma_{NO_3} \qquad (5)$$

Below 248 nm, $\Phi_{NO_3}^{N_2O_5}$ approaches unity rapidly.[17] In our previous work, we assumed $\Phi_{NO_3}^{N_2O_5} = 1.0 \pm 0.10$ and we propagate the same assumed error in our current analysis. The precursor number density is measured upstream from the photolysis chamber by an FTIR spectrometer (Perkin-Elmer Paragon 1000). The precursor number densities ($\tilde{N}_{PAN,N_2O_5}$) are combined with the absorption cross sections (σ_{PAN,N_2O_5}), and photolytic number densities $[NO_3]_{PAN,N_2O_5}$ to extract the quantum yield as follows.

$$\Phi_{NO_3}^{PAN} = \Phi_{NO_3}^{N_2O_5} \times \frac{[NO_3]_{PAN}}{[NO_3]_{N_2O_5}} \times \frac{\sigma_{N_2O_5}}{\sigma_{PAN}} \times \frac{\tilde{N}_{N_2O_5}}{\tilde{N}_{PAN}} \qquad (6)$$

The synthesis of PAN followed the report of Gaffney et al.[18] and N_2O_5 was synthesized according to Davidson et al.[19] Estimates of impurities in the precursor samples were performed by FTIR analysis and found negligible. Both PAN and N_2O_5 samples were used without further purification. Our previous study included a photolysis power dependence study for N_2O_5 between 0.0 and 2.0 mJ.[11] We find the signal to be linear in power up to 2.0 mJ and use increasing photolysis power to overcome a decreasing PAN absorption cross section in this region.[20,21] We used a photolysis energy of 1.0 mJ for the experiments at 289, 294, and 299 nm, 1.5 mJ at 308 nm, and 1.6 mJ at 312 nm, thereby staying well within the one-photon photolysis range for the reference gas. We assume the same power dependence for PAN photolysis. For these relative quantum yield experiments, N_2O_5 is introduced to the chamber at 10 Torr and 0.1 SLPM flow rate for N_2 carrier gas. Following an experiment, the chamber is evacuated, the carrier gas flow is switched to the PAN sample, then the CRDS scan is performed again. Another sequence is performed using N_2O_5 to bracket the PAN experiment. The precursor number density ($\tilde{N}$) for PAN and N_2O_5 is measured four times during the CRDS scan. The precursor concentrations are normalized to their value when the CRDS laser is at 662 nm. The Δr spectrum is fit to the precursor decay profile to normalize the spectrum by the normalized $\tilde{N}$ decay.

A local version of the ACES II quantum chemistry program was used in this study.[22] The ground state geometries were optimized for $HOONO_2$ using CCSD/DZP and CCSD/cc-pVTZ calculations, and CCSD/DZP calculations were used for PAN. Harmonic vibrational analysis indicated that all structures were global minima on the respective potential energy surface. The vertical excitation energy (VEE) calculations were performed using the equation of motion coupled cluster singles and doubles (EOM-CCSD) method.[23] The oscillator strengths (f) for the respective electronic transitions are calculated by

$$f_{eg} = 4.702 \times 10^{-7}\ (\text{cm D}^{-2})\ \nu_{eg}|\mu_{eg}|^2 \qquad (7)$$

where ν_{eg} is the transition energy in cm^{-1} and μ_{eg} is the transition dipole moment in Debye. In addition to the VEE analysis, the energy gradients for the internal coordinate representations of each species in each 1−4 ^{1}A electronic states are calculated. The energy gradients are obtained by performing geometry optimizations of each 1−4 ^{1}A electronic excited states, again using the EOM-CCSD method. The optimizations are stopped after one cycle to estimate the gradients along internal coordinates due to electronic excitation. Bonds elongated from their r_e position in the ground state have negative energy gradients. Therefore, internal coordinates with large negative energy gradients are stretched in each excited state and those with positive gradients are compressed. By performing this analysis

TABLE 1: Number Densities and Quantum Yields for PAN/N_2O_5 Photolysis Experiments between 289 and 312 nm[a]

expt no.	$[N_2O_5]$	[PAN]	NO_3 ratio	$\Phi^{PAN}_{NO_3}$
		289 nm		
1	1.30 ± 0.10	6.49 ± 0.89	0.14 ± 0.01	0.34 ± 0.10
2	2.37 ± 0.02	2.77 ± 0.03	0.23 ± 0.01	0.24 ± 0.01
3	1.31 ± 0.10	3.37 ± 0.19	0.08 ± 0.01	0.36 ± 0.08
4	8.37 ± 0.18	2.76 ± 0.02	0.08 ± 0.01	0.29 ± 0.04
5	5.43 ± 0.51	5.81 ± 1.50	0.024 ± 0.002	0.32 ± 0.10
6	4.44 ± 0.42	4.28 ± 0.55	0.024 ± 0.001	0.29 ± 0.07
		294 nm		
1	2.17 ± 0.01	4.18 ± 0.04	0.03 ± 0.003	0.25 ± 0.02
2	3.99 ± 0.02	28.1 ± 0.02	0.18 ± 0.005	0.31 ± 0.02
3	2.36 ± 0.001	8.55 ± 0.02	0.09 ± 0.004	0.28 ± 0.03
4	1.42 ± 0.007	2.44 ± 0.007	0.030 ± 0.001	0.33 ± 0.03
5	2.31 ± 0.01	46.7 ± 2.0	0.37 ± 0.01	0.27 ± 0.1
6	1.49 ± 0.03	30.6 ± 0.3	0.40 ± 0.02	0.29 ± 0.2
7	1.54 ± 0.02	11.1 ± 0.1	0.09 ± 0.02	0.31 ± 0.08
8	1.88 ± 0.10	27.0 ± 2.0	0.30 ± 0.01	0.31 ± 0.04
		299 nm		
1	2.73 ± 0.02	5.20 ± 0.02	0.03 ± 0.01	0.29 ± 0.05
2	2.06 ± 0.02	23.3 ± 0.30	0.15 ± 0.01	0.28 ± 0.03
3	2.46 ± 0.02	33.0 ± 1.0	0.16 ± 0.01	0.27 ± 0.02
4	2.46 ± 0.02	11.0 ± 0.2	0.04 ± 0.01	0.20 ± 0.03
5	2.87 ± 0.03	14.2 ± 0.002	0.08 ± 0.01	0.36 ± 0.02
6	1.75 ± 0.03	43.2 ± 0.80	0.32 ± 0.01	0.28 ± 0.02
7	1.43 ± 0.04	14.1 ± 0.10	0.14 ± 0.01	0.30 ± 0.03
		308 nm		
1	2.48 ± 0.01	31.6 ± 4.0	0.07 ± 0.01	0.17 ± 0.05
2	1.58 ± 0.01	37.8 ± 0.70	0.28 ± 0.01	0.34 ± 0.02
3	1.66 ± 0.03	11.5 ± 1.0	0.05 ± 0.01	0.24 ± 0.05
4	1.52 ± 0.01	13.5 ± 0.60	0.08 ± 0.01	0.28 ± 0.04
5	2.20 ± 0.01	16.8 ± 0.04	0.08 ± 0.01	0.33 ± 0.02
6	1.53 ± 0.04	52.5 ± 0.08	0.37 ± 0.01	0.32 ± 0.02
7	1.70 ± 0.05	14.4 ± 0.04	0.08 ± 0.02	0.27 ± 0.08
		312 nm		
1	1.91 ± 0.02	15.4 ± 0.007	0.10 ± 0.01	0.44 ± 0.06
2	1.67 ± 0.02	27.0 ± 0.001	0.17 ± 0.01	0.39 ± 0.11
3	1.54 ± 0.001	7.42 ± 0.15	0.06 ± 0.01	0.43 ± 0.08
4	2.42 ± 0.06	13.3 ± 0.005	0.04 ± 0.01	0.29 ± 0.04
5	1.59 ± 0.03	34.9 ± 0.04	0.26 ± 0.02	0.43 ± 0.04
6	2.20 ± 0.02	28.0 ± 0.05	0.15 ± 0.01	0.43 ± 0.04
7	1.56 ± 0.02	34.1 ± 3.60	0.21 ± 0.02	0.35 ± 0.07
8	2.39 ± 0.01	52.1 ± 0.10	0.20 ± 0.01	0.34 ± 0.03

[a] The number densities are reported $\times 10^{14}$ molecule cm^{-3}. The uncertainties for the number densities are 2σ. The photolytic NO_3 ratio and associated error are described in the text.

with the DZP and pVTZ basis sets on $HOONO_2$, we are able to qualitatively infer the effects of photoexcitation on the bare $-OONO_2$ chromophore and the quality of the DZP results. The calculations are extended to PAN using only the DZP basis set.

III. Results and Discussion

Table 1 contains the normalized precursor number densities $\tilde{N}$ for PAN and, N_2O_5, the ratio of photolytic NO_3 from PAN and N_2O_5 photolysis, UV absorption cross sections, and the derived quantum yield for each experiment at each photolysis wavelength. The $\Phi^{PAN}_{NO_3}$ measurements depend on measuring the precursor number densities and Δr as accurately as possible. Previous work indicates our photolysis measurement has a detection limit of 2×10^7 molecule cm^{-3}.[11] A photolytic difference spectrum for PAN photolysis at 312 nm is shown in Figure 1. The open circles are the difference (Δr) measured between photolysis off and on states converted to NO_3 absorption spectrum. The solid line represents the reference spectrum reported in the JPL reference, though scaled to $\sigma_{NO_3}(662\text{ nm}) = 2.1 \times 10^{-19}$.[16] By quantifying the photolytic number density measurement with a reference spectrum, we ensure that the photoproduct measured represents the absorption of NO_3 with no significant photochemical impurity.

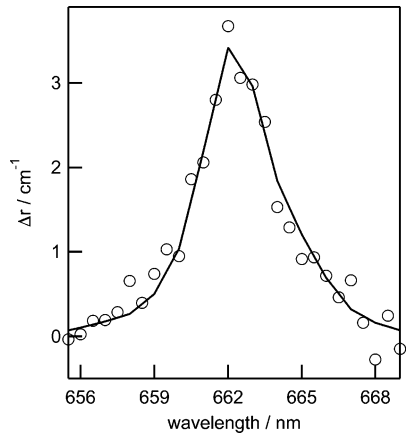

Figure 1. Photolysis difference spectrum taken during PAN photolysis at 312 nm. The open circles are those derived from eq 5. The solid line is the nitrate radical reference spectrum from the JPL reference.[16]

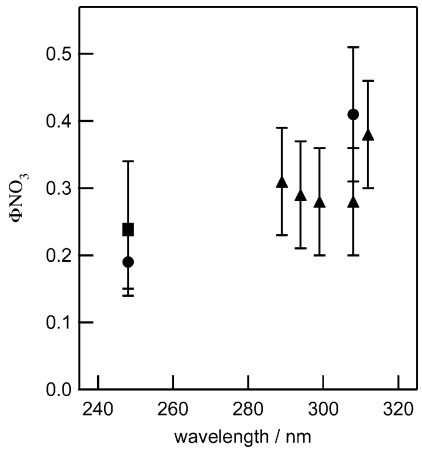

Figure 2. Nitrate radical quantum yields from PAN photolysis plotted vs wavelength. The square is the data from Mazely et al.,[10] the circle is data from Harwood et al.,[8] and the triangles are the results of our experiments at 289, 294, 299, 308, and 312 nm. The error bars are $\pm 2\sigma$ in accordance with the data in Table 1.

The wavelength dependence of $\Phi^{PAN}_{NO_3}$ measured from these experiments is shown in Figure 2. Our measurements of $\Phi^{PAN}_{NO_3}$ are indicated by the solid triangles at 289 nm[11] (0.31 ± 0.07), 294 mn (0.29 ± 0.07), 299 nm (0.28 ± 0.07), 308 nm (0.28 ± 0.05), and 312 nm (0.39 ± 0.07). Additional data points are shown for the experiments of Mazely et al.[10] at 248 nm (solid box), and the study of Harwood et al.[8] at 248 and 308 nm (solid circle). We can directly compare our result at 308 nm with that of Harwood et al. and find the values to be within experimental uncertainty. Our experimental results indicate that, at least between 290 and 308 nm, $\Phi^{PAN}_{NO_3}$ is not increasing and is equal to 0.29, on averaging the $\Phi^{PAN}_{NO_3}$ results at 289, 294, 299, and 308 nm. Our data at 308 and 312 nm are in experimental agreement, though an increase in $\Phi^{PAN}_{NO_3}$ at even longer wavelengths cannot be ruled out. This fluctuation at the longer wavelengths in our data is potentially due to more uncertainty in the measurement of photolytic NO_3 from PAN photolysis. At the weakest absorbing photolysis wavelength used here ($\sigma_{PAN} = 5.40 \times 10^{-22}$ cm^2 $molecule^{-1}$), we detect an average of (1.2 ± 0.7) × 10^9 molecule cm^{-3} NO_3 for our eight experiments. The same statistic for the 289 nm photolysis of PAN is (3.9 ±

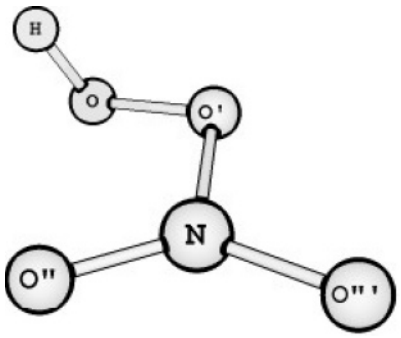

Figure 3. Peroxy nitric acid (PNA) structure used in current study.

0.10) $\times$ 10^9 molecule cm^{-3} NO_3 ($\sigma_{PAN} = 5.95 \times 10^{-21}$ cm^2 $molecule^{-1}$). As σ_{PAN} decreases, we are detecting a smaller and relatively more uncertain amount of NO_3. Considering the behavior of σ_{PAN} with wavelength, it is unlikely that at wavelengths beyond 312 nm that $\Phi_{NO_3}^{PAN}$ would still be increasing. For atmospherically relevant photolysis wavelengths, it is appropriate to consider $\Phi_{NO_3}^{PAN} = 0.30$.

To understand better our theoretical results for PAN excited states and quantum yields, we have also performed excited state calculations for peroxy nitric acid (PNA) and compared our theoretical results with the recently reported experimental measurements of PNA photolysis quantum yields reported by Jimenez et al.[6] and in the work by Roehl et al.[7] Peroxy nitric acid is the simplest species containing the $-OONO_2$ moiety and has a ground state molecular orbital configuration of $(1-17)a^2 18a^2 19a^2 20a^2$ with C_1 symmetry. There have been previous calculations of the vertical excitation energies for PNA, with which our calculations agree quite well. The work presented by Roehl et al.[7] indicates two PNA singlet excited states resulting from $n \rightarrow \pi^*$ excitations at 5.05 and 5.52 eV (MRCI/cc-pVDZ). Roehl et al. also report potential energy surfaces for low lying 2 ^{1}A and 3 ^{1}A states calculated as a function internuclear separation along the dissociated O−O and O−N bond coordinates. These potential surfaces indicated predissociative surfaces calculated along the O−N coordinate cross within the Franck−Condon region (within $\pm$0.25 Å of the equilibrium bond length), whereas the curve crossings along the O−O coordinate occur at further separations. By virtue of the curves crossing at smaller separation, i.e., closer to the r_e value, the O−N coordinate dissociates more readily, which is reflected in their NO_2 quantum yield measurement at 248 nm of 0.56 ± 0.17.[7] The NO_2 quantum yield of Roehl et al. is in agreement with the HO_2 quantum yield measurement of Jimenez et al. of 0.89 ± 0.26,[6] confirming at 248 nm that (3) dominates PNA photolysis at 248 nm.

We have calculated the structure for PNA using both CCSD/DZP and CCSD/cc-pVTZ methods. The resulting structure is in excellent agreement with the high level analysis of the PNA global minimum strucuture reported by Matthews et al.[24] For reference, a ball and stick representation of our PNA structure is shown in Figure 3. In our work we identify the same 2 ^{1}A and 3 ^{1}A excited states at 5.35 and 6.11 eV, resulting from 18a and 19a $\rightarrow$ 21a excitations, shown in Table 2. The 18a and 19a MOs correspond to O−O′ and O′−N bonding orbitals and 21a is a π^* antibonding MO in $-NO_2$. Table 2 indicates relatively weak oscillator strengths for these transitions: $f = 3.8 \times 10^{-5}$ and 3.9×10^{-4}, respectively. Therefore, the first two excited states, though weakly absorbing, promote the respective electron into the anitbonding 21a orbital and lead to dissociation of the HOO′−NO_2 bond. Presumably as photon energies decrease to the UV−B wavelengths, (3) will continue to be the dominant $HOONO_2$ photolysis pathway.

TABLE 2: Vertical Excitation Energies (eV) and Oscillator Strengths for $HOONO_2$ and PAN[a]

	transition	DZP	cc-pVTZ	f
$HOONO_2$	2 ^{1}A → 1 $^1\tilde{X}$ (18a → 21a)	5.14	5.35	3.8×10^{-5}
	3 ^{1}A → 1 $^1\tilde{X}$ (19a → 21a)	5.87	6.11	3.9×10^{-4}
	4 ^{1}A → 1 $^1\tilde{X}$ (20a → 21a)	7.05	7.30	1.9×10^{-3}
$CH_3C(O)OONO_2$	2 ^{1}A → 1 $^1\tilde{X}$ (28a → 32a)	5.22		5.2×10^{-6}
	3 ^{1}A → 1 $^1\tilde{X}$ (29a → 32a)	5.98		3.2×10^{-4}
	4 ^{1}A → 1 $^1\tilde{X}$ (31a → 33a)	6.07		1.9×10^{-3}
	5 ^{1}A → 1 $^1\tilde{X}$ (30a → 32a)	7.15		0.24

[a] The f values are calculated using the DZP basis set.

The dissociation of the O′−O and O′−N bonds in Figure 3 is responsible for the formation of either [HO + ONO_2] or [HO_2 + NO_2] from PNA. Therefore the energy gradient for these coordinates in each of the ^{1}A excited states is of interest. The energy gradients for these and other bonding internal coordinates for each excited state are included as Supporting Information. For PNA, we calculate the gradients using both the DZP and cc-pVTZ basis sets, observe little difference between the DZP and cc-pVTZ energy gradients, and are confident the DZP results accurately describe the energy gradients upon excitation. In the 2 ^{1}A excited state, the terminal N−O″ and N−O‴ bonds are stretched, and there is a minimal energy gradient predicted for either the O−O′ or O′−N bonds. The same is found for the 3 ^{1}A excited state. Hence, for the first two excited states of PNA, the terminal $-NO_2$ bonds are stretched. The redistribution of this energy causes the relatively weak O′−N bond (24 kcal mol^{-1}) to dissociate. The O−O′ bond is stronger (39 kcal mol^{-1}) and is dissociated to a much lesser extent. This is evident in the experimental results of Jimenez et al. where $\Phi_{NO_3}^{PNA} = 0.08$ and 0.05 at 248 and 308 nm.[6]

We have extended our calculations to the third singlet excited state of PNA as well. The 4 ^{1}A state corresponds to the 20a $\rightarrow$ 21a excitation between the nonbonding HOMO of the terminal $-NO_2$ group and the LUMO π^* $-NO_2$ orbital. Here, we predict a much larger transition energy of 7.3 eV with an oscillator strength of $f = 0.125$. The energy gradients in the 4 ^{1}A state indicate the N−O″ and O−O″ bonds are stretched and the second N−O‴ bond is stretched to a lesser extent. The situation is similar to that of the previous excited states in that the terminal $-NO_2$ group is affected, but due to the additional excitation of the O−O stretch, there is a competition between dissociation reactions 1 and 2. The excitation of the O−O′ bond presumably leads to dissociation production [HO + ONO_2]. The results of Jimenez et al. at 193 nm indicate the NO_3 quantum yield is 0.35 ± 0.09. This enhancement in the NO_3 quantum yield, relative to $\Phi_{NO_3}^{PNA}$ at 248 and 308 nm, is possibly due to competition between direct O−O bond rupture and the redistribution of energy partitioned into the terminal $-NO_2$ bonds.

The characterization of these three excited states in PNA are relevant when considering the photoexcitation of PAN. The VEE and energy gradient calculations and experimental results for PNA have provided a clear picture of the photochemistry of the bare $-OONO_2$ moiety. The low lying $n \rightarrow \pi^*$ transitions of PNA have small oscillator strengths, and the transition energy and oscillator strengths of the analogous transitions in the photoexcitation on PAN are of interest in characterizing the primary excitations involved in its atmospheric photolysis. Additionally, the presence of the carbonyl bond in the acetyl moiety will have its own $n \rightarrow \pi^*$ transition. A significant red shift of the third $-OONO_2$ state could also account for the

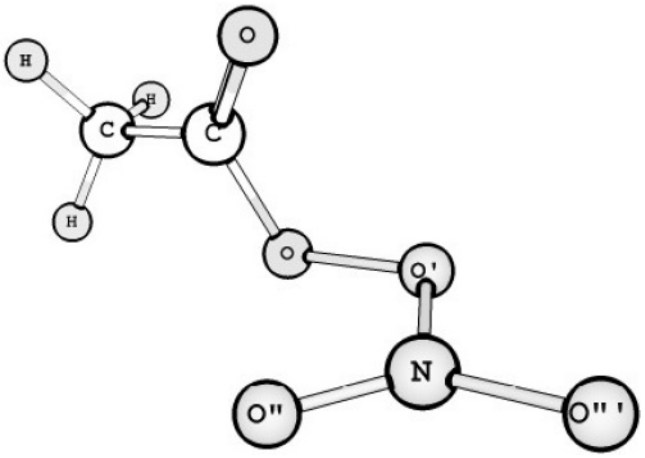

Figure 4. Peroxyacetyl nitrate (PAN) structure used in current study.

enhanced Φ_{NO_3} in PAN relative to PNA. The excited state energy gradient calculations are also helpful to characterize the dissociation of PAN.

All calculations on PAN were performed using CCSD/DZP. The results for the structure are similiar to the CCSD[T]/cc-pVDZ results reported by Francisco and Li.[15] A ball and stick picture of our PAN structure is shown in Figure 4. The vertical excitation and oscillator strength results for PAN excited states are also presented for direct comparison to PNA in Table 2. The PAN ground state has C_1 symmetry and a 1-31a^2 molecular orbital configuration. We have identified the same primary n to π^* (28a $\rightarrow$ 32a, 29a $\rightarrow$ 32a) transitions as in PNA and an additional n $\rightarrow \pi^*$ transition involving the C═O group present in the acetyl moiety (31a $\rightarrow$ 33a). The 28a and 29a MOs are mixed with O−O′ and O′−N bonding character and $-NO_2$ nonbonding character, respectively. Therefore transitions from these orbitals are analogous to the low lying 2 and 3 ^{1}A excited states of PNA. The acetyl group does relatively little to change the location of the three $-OONO_2$ n $\rightarrow \pi^*$ and $\pi \rightarrow \pi^*$ excited states in PAN. We calculate these energies at 5.22, 5.98, and 7.15 eV (compared to 5.14, 5.87, and 7.05 eV for PNA) using EOM-CCSD/DZP at the CCSD/DZP optimized geometry for PAN. Hence, the first two n $\rightarrow \pi^*$ transitions are blue-shifted in PAN by ca. 0.1 eV relative to PNA and the third n $\rightarrow \pi^*$ transition is red-shifted by ca. 0.1 eV. We calculate the n $\rightarrow \pi^*$ transition of the C═O molecular orbitals at 6.07 eV. The oscillator strengths for the PAN transitions also show little change for the 2 and 3 ^{1}A transitions of the $-OONO_2$ chromophore. The 4 ^{1}A state corresponding to the C═O transition is predicted to be an order of magnitude larger than the 2 and 3 ^{1}A states. The strongest transition in PAN is calculated for the third n $\rightarrow \pi^*$ transition (30a $\rightarrow$ 32a). This is the third state correlating to the $-OONO_2$ group in PAN. It is calculated to be another 2 orders of magnitude stronger than the 4 ^{1}A $\rightarrow$ 1 $^1\tilde{X}$ transition. The three $-OONO_2$ transitions in PAN are of similar intensity to the same transitions in PNA. Only the 2 ^{1}A state varies in predicted intensity, it is predicted to be an order of magnitude smaller in PAN than in PNA. The $-OONO_2$ electronic excited states in PAN and PNA are very similar and apparently unaffected by the presence of the acetyl group in PAN.

The internal coordinates in PAN of interest are the O−O′ and O′−N bonds, as well as the terminal $-NO_2$ bonds. Additionally, any excitation of the C═O and C−O bonds of PAN will be important factors due to the absorption of the carbonyl moiety of PAN. In the 2 and 3 ^{1}A states of PAN, the terminal $-NO_2$ bonds are excited as they are in the 2 and 3 ^{1}A states of PNA. In the 3 ^{1}A state, the O′−N bond is stretched significantly as well. Thus, the first two excited states of PAN are completely analagous to those of PNA; the terminal $-NO_2$ bonds are stretched in the absorption by the $-NO_2$ chromophore and that energy is redistributed to break weakest bond in the molecule. The 4 ^{1}A state of PAN is dominated by the C═O absorption. The largest energy gradient predicted in this state is for the C═O bond and the C−O bond. Also, the O−O′ bond is stretched in this state, whereas it had been compressed in the previous two excited states. This is a direct excitation of the coordinate responsible for reaction 4, though there is more energy deposited in the O′−N coordinate responsible for reaction 3. The 4 ^{1}A state absorbs strongly ($f = 0.0019$), so it is likely that this transition is excited by solar radiation.

The final state considered here is the 5 ^{1}A state of PAN. This state has the largest oscillator strength of any in this study ($f = 0.24$) and nearly every coordinate is excited to a relatively large degree. With the exception of the excitation of the C−O and O−O′ bonds, this state is similar to the 4 ^{1}A state for PNA. The internal coordinate results show the elongation of one terminal $-NO_2$ bond. The O′−N bond is excited in this state as well as the O−O′ bond, and both coordinates have their largest repulsive gradients in this state. Thus, the situation for PAN photoexcitation is similar to that of PNA, with the two lowest states due to $-NO_2$ n to π^* orbital excitations.

It appears then that the acetyl group of PAN has little effect in terms of providing a direct mechanism for the increase in Φ_{NO_3} for PAN relative to PNA. The carbonyl bond absorbs radiation in the 4 ^{1}A state, but there is little direct excitation of O−O′ bonding orbitals accompanying this relatively strong excitation. The other states in PAN are like PNA, the excitation primarily affects the terminal NO bonds and the energy redistributes to break either the O−O or O−N bonds to produce NO_3 or NO_2 (and the corresponding organic radical), respectively. The difference, then, can be attributed to a smaller gap between the bond energies of O−O′ and O′−N in PAN relative to PNA. Because there is no evidence for a direct dissociation of either coordinate in either molecule, the differences in the thermochemistry of the dissociation reactions could be the cause for the differences in the observed photochemical behavior. In PAN, the thermochemistry of the reactions producing NO_3 and NO_2 are much less certain than for the reaction enthalpies of PNA. An estimate of the differences in reactions 1−4 was reported by Miller et al.[14] using the *ab initio* model chemistry CBS-Q to estimate the difference in $\Delta_{rxn}H$ between reactions (1) and (2) of 17.6 kcal mol^{-1}. Our own estimate from current experimental results is 19.6 ± 1 kcal mol^{-1}, assuming Δ_fH(298 K) $HOONO_2 = -12.6 \pm 1.0$ kcal mol^{-1},[25] Δ_fH(298 K, NO_2) = 8.12 ± 0.01,[26] and Δ_fH(298 K, HO_2) = 2.94 ± 0.06 kcal mol^{-1},[26] Δ_fH(298 K, NO_3) = 17.6 ± 0.3,[27] and Δ_fH(298 K, OH) = 8.93 ± 0.01.[26] In PAN, the difference in reaction enthalpies for the NO_2 and NO_3 producing channels was calculated by Miller et al. to be 6.9 kcal mol^{-1} (CBS-Q). We estimate the same difference experimental results of 10.3 kcal mol^{-1}, assuming the same Δ_fH(298 K) for NO_2 and NO_3 as before, Δ_fH(298 K, $CH_3C(O)O$) = −41.0 ± 3 kcal mol^{-1},[12] Δ_fH(298 K, $CH_3C(O)OO$) = −41.1 ± 5 kcal mol^{-1},[28] and Δ_fH(298 K, PAN) = −57 ± 5 kcal mol^{-1}.[28] Therefore the differences between reaction enthalpies for the two decomposition channels in PAN are closer than those for PNA, resulting in more NO_3 being produced by its photolysis.

IV. Conclusions

We have measured the nitrate radical quantum yield from peroxyacetyl nitrate photolysis at several wavelengths relevant

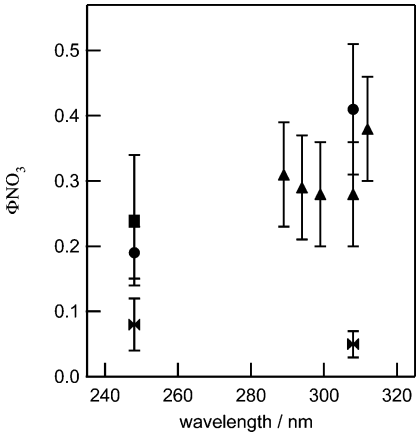

Figure 5. Nitrate radical quantum yields for PAN *and* PNA photolysis, plotted vs wavelength. Compared to Figure 2, the additional bowtie data are for PNA photolysis reported by Jimenez et al.[6] The data show the difference in Φ_{NO_3} between the two molecules, where $= \Phi_{NO_3}^{PAN} =$ 0.30 and $\Phi_{NO_3}^{PNA} \leq 0.10$.

for atmospheric photolysis. Between 289 and 308 nm we measure $\Phi_{NO_3}^{PAN}$ to be $\sim 0.30 \pm 0.07$. At 312 nm, we measure $\Phi_{NO_3}^{PAN}$ to be 0.39 ± 0.07. This discrepancy is most likely related to reduced accuracy in the photolytic NO_3 measurement at 312 nm where the production of NO_3 from PAN photolysis is lowest, though we note that the results are still within experimental agreement. It would be beneficial to carry on these measurements at photolysis wavelengths approaching 320 nm to further define the trend in $\Phi_{NO_3}^{PAN}$ with wavelength. In addition to the experimental studies, we have investigated the photochemistry involved in PAN and PNA photolysis using EOM-CCSD quantum chemical calculations of the excited state energies, oscillator strengths, and energy gradients. We find that photodissociation of PAN occurs via excitation to predissociative excited states and the redistribution of that energy breaks both the O−O and O−N bonds of PAN, as opposed to a directly dissociative transition that might be affected by the photolysis wavelength. The excited states in the reference molecule PNA translate closely to three of the four states investigated for PAN photolysis. The related states in both molecules correspond to $n \rightarrow \pi^*$ excitations on the $-OONO_2$ chromophore. The remaining state in PAN corresponds to the carbonyl group in the acetyl side of the molecule, which is of course absent in PNA. Due to similarities in the effect of photoexcitation predicted for both PAN and PNA, we determined differences in bond energies for the NO_2 and NO_3 producing channels (reactions 1−4) are responsible for the observed and striking difference in NO_2 and NO_3 quantum yields for these molecules (Figure 5). Further studies in the class of organic peroxy nitrates $ROONO_2$ should provide a needed picture of the photolysis and thermolysis of these atmospherically relevant RO_x and NO_x reservoir species.

Supporting Information Available: Tables of excited state energy gradients. This material is available free of charge via the Internet at http://pubs.acs.org.

References and Notes

(1) Roberts, J. M. *Atmos. Environ.* **1990**, *24A*, 243.
(2) Moxim, W. J.; Levy, H., II; Kasibhatla, P. S. *J. Geophys*. Res. **1996**, *101*, 12621.
(3) Macleod, H.; Smith, G. P.; Golden, D. M.; J. *Geophys. Res.* **1988**, *93*, 3813 and references cited within.
(4) Matthews, J.; Sharma, R.; Sinha, A. *J. Phys. Chem. A* **2004**, *108*, 8134.
(5) Roehl, C. M.; Nizkorodov, S. A.; Zhang, H.; Blake, G. A.; Wennberg, P. O. *J. Phys. Chem.* **2002**, *106*, 3766.
(6) Jimenez, E.; Gierczak, T.; Stark, H.; Burkholder, J. B.; Ravishankara, A. R. *Phys. Chem. Chem. Phys.* **2005**, *7*, 432.
(7) Roehl, C. M.; Mazely, T. L.; Freidl, R. R.; Li, Y.; Francisco, J. S.; Sander, S. P. *J. Phys. Chem. A* **2001**, *105*, 1592.
(8) Harwood, M.; Roberts, J.; Frost, G.; Ravishankara, A.; Burkholder, J. *J. Phys. Chem. A* **2003**, *107*, 1148.
(9) Mazely, T.; Freidl, R.; Sander, S. *J. Phys. Chem.* **1995**, *99*, 8612.
(10) Mazely, T.; Freidl, R.; Sander, S. *J. Phys. Chem. A* **1997**, *101*, 7090.
(11) Flowers, B. A.; Angerhofer, M. E.; Simpson, W. R.; Nakayama, T.; Matsumi, Y. *J. Phys. Chem.* **2005**, *109*, 2552.
(12) Blanksby, S. J.; Ellison, G. B. *Acc. Chem. Res.* **2003**, *36*, 255.
(13) Orlando, J.; Tyndall, G.; Calvert, J. *Atmos. Environ.* **1992**, *26A*, 3111.
(14) Miller, C. E.; Lynton, J. I.; Keevil, D. M.; Francisco, J. S. *J. Phys. Chem. A* **1999**, *103*, 11451.
(15) Francisco, J. S.; Li, Y. *J. Chem. Phys.* **2004**, *121*, 6298.
(16) Sander, S. P.; Freidl, R. R.; Golden, D. M.; Kurylo, M. J.; Huie, R. E.; Orkin, V. L.; Moortgat, G. K.; Ravishankara, A. R.; Kolb, C. E.; Molina, M. J.; Finlayson-Pitts, B. J. *Chemical Kinetics and Photochemical Data for Use in Atmospheric Studies*; Evaluation 14, Publication 02-25; NASA/Jet Propulsion Laboratory: Pasadena, CA, 2003 (see also references cited within).
(17) Harwood, M.; Burkholder, J.; Ravishankara, A. *J. Phys. Chem. A* **1998**, *102*, 1309 and references cited within.
(18) Gaffney, J.; Fajer, R.; Senum, G. *Atmos. Environ.* **1984**, *18*, 215.
(19) Davidson, D.; Viggiano, A.; Howard, C.; Dotan, L.; Fehsenfeld, F.; Albritton, D.; Ferguson, E. *J. Chem. Phys.* **1978**, *68*, 2085.
(20) Talukdar, R.; Burkholder, J.; Schmolter, A.; Roberts, J.; Wilson, R.; Ravishankara, A. *J. Geophys. Res.* **1995**, *100*, 14163.
(21) Senum, G.; Lee, Y.; Gaffney, J. *J. Phys. Chem.* **1984**, *88*, 1269.
(22) Stanton, J. F.; Gauss, J.; Watts, J. D.; Lauderdale, W. J.; Bartlett, R. J. *Int. J. Quantum Chem. Symp*. **1992**, *26*, 879.
(23) Stanton, J. F. Bartlett, R. J. *J. Phys. Chem.* **1993**, *98*, 7029.
(24) Matthews, J.; Sinha, A.; Francisco, J. S. *J. Chem. Phys.* **2004**, *121*, 5720.
(25) Gierczak, T.; Jimenez, E.; Riffault, V.; Burkholder, J.; Ravishankara, A. R. *J. Phys. Chem. A* **2005**, *109*, 586.
(26) Ruscic, B.; Pinzon, R. E.; Morton, M. E.; Srinivasan, N. K.; Su, M.; Sutherland, J. W.; Michael, J. V. *J. Phys. Chem. A*, submitted for publication.
(27) Davis, H. F.; Kim, B.; Johnston, H. S.; Lee, Y. T. *J. Phys. Chem.* **1993**, *97*, 2171.
(28) Bridier, I.; Caralp. F.; Loriat, H.; Lesclaux, R.; Veyret, B.; Becker, K.; Reimer, A.; Zabel, F. *J. Phys. Chem.* **1991**, *95*, 3594.